Geophys. J. Int. (2007) **169,** 733–746 doi: 10.1111/j.1365-246X.2007.03342.x

Neural network modelling and classification of lithofacies using well log data: a case study from KTB borehole site

Saumen Maiti,[1] Ram Krishna Tiwari[1] and Hans-Joachim Kümpel[2]

[1]*Mathematical Modelling Group, National Geophysical Research Institute, Hyderabad* 500007, *India. E-mail: saumen_maiti2002@yahoo.co.in*
[2]*GGA-Institut (Leibniz Institute for Applied Geosciences), Stilleweg* 2 D-30655 *Hannover, Germany*

Accepted 2006 December 29. Received 2006 December 29; in original form 2004 October 14

SUMMARY

A novel approach based on the concept of super self-adapting back propagation (SSABP) neural network has been developed for classifying lithofacies boundaries from well log data. The SSABP learning paradigm has been applied to constrain the lithofacies boundaries by parameterzing three sets of well log data, that is, density, neutron porosity and gamma ray obtained from the German Continental Deep Drilling Project (KTB). A multilayer perceptron (MLP) neural networks model was generated in a supervised feed-forward mode for training the published core sample data. A total of 351 pairs of input and output examples were used for self-adaptive network learning and weight and bias values were appropriately updated during each epoch according to the gradient-descent momentum scheme. The actual data analysis suggests that the SSABP network is able to emulate the pattern of all three sets of KTB data and identify lithofacies boundaries correctly. The comparisons of the maximum likelihood geological sections with the available geological information and the existing geophysical findings over the KTB area suggest that, in addition to the known main lithofacies boundaries units, namely paragneisses, metabasites and heterogeneous series containing partly calc-silicate bearing paragneisses-metabasites and alternations of former volcano-sedimentary sequences, the SSABP neural network technique resolves more detailed finer structures embedded in bigger units at certain depths over the KTB region which seems to be of some geological significance. The efficacy of the method and stability of results was also tested in presence of different levels of coloured noise. The test results suggest that the designed network topology is considerably unwavering for up to 20 per cent correlated noise; however, adding more noise (∼50 per cent or more) degrades the results. Our analyses demonstrate that the SSABP based approach renders a robust means for the classification of complex lithofacies successions from the KTB borehole log data and thus may provide useful guide/information for understanding the crustal inhomogeneity and structural discontinuity in many other regions.

Key words: ANN, back propagation method, KTB boreholes, lithofacies, petrophysics, well log.

INTRODUCTION

One of the main goals of geophysical studies is to apply suitable mathematical and statistical techniques to extract information about the subsurface properties (e.g. lithology, porosity, density, hydraulic conductivity, resistivity, salinity and water/oil saturation) by using either the surface or borehole measurements (Aristodemou *et al.* 2005). In particular, classification of lithofacies boundaries using the geophysical well log data is quite important from the oil exploration point of view as well as for understanding the crustal inhomogeneity. Geoscientists have been engaged in classifying lithofacies units from the recorded well log data using the conventional method like graphical cross-plotting and other statistical techniques (Rogers *et al.* 1992). In the graphical cross-plotting technique (Pickett 1963; Gassaway *et al.* 1989), two or more logs are cross-plotted to yield lithologies. Multivariate statistical methods such as principle component and cluster analyses (Wolff & Pelissier-Combescure 1982) and discriminant function analysis (Busch *et al.* 1987; Delfiner *et al.* 1987) have invariably been used for the study of borehole data. These techniques are, however, semi-automated and require a large amount of data, which are costly and not easily available every time (Rogers *et al.* 1992). Further the existing methods for well log data analysis are also very tedious and time-consuming, particularly when dealing with noisy and complex borehole data. In fact, classifying litho log boundary from borehole data is a complex and non-linear problem. This is due to the fact that several factors, such as pore fluid,

© 2007 The Authors
Journal compilation © 2007 RAS

effective pressure, fluid saturation, pore shape, etc. affect the well log signals and thereby limit the applicability of linear mathematical techniques to classify lithofacies units. It is, therefore, imperative to search for an appropriate non-linear technique, which could evade these difficulties. The modern data modelling approach based on the artificial neural network (ANN) techniques is inherently non-linear and completely data-driven requiring no initial model and hence provide an effective alternative approach to deal with such a complex and non-linear geophysical problem (Saggaf *et al.* 2003).

Recently, the ANN based techniques have been widely applied in almost all branches of geophysics (Van der Baan & Jutten 2000; Poulton 2001). For example: (1) for seismic event classification (Dysart & Pulli 1990; Dai & Macbeth 1995; Yin-ju 2002), (2) well log analysis (Baldwin *et al.* 1990; Rogers *et al.* 1992; Huang *et al.* 1996; Helle *et al.* 2001; Zhan *et al.* 2002; Aristodemou *et al.* 2005), (3) first arrival picking (Murat & Rudman 1992; McCormack *et al.* 1993), (4) earthquake prediction (Feng *et al.* 1997), (5) inversion (Raiche 1991; Roth & Tarantola 1994; Boadu 1998; Devilee *et al.* 1999; Aristodemou *et al.* 2005), (6) parameter estimation in geophysics (Calderon-Macias *et al.* 2000) and (7) prediction of aquifer water level (Coppola *et al.* 2005, etc.). The ANN techniques have also become increasingly popular for signal detection and data compression. In particular, ANN based approaches have proved to be one of the robust and cost-effective alternative means to successfully resolve the lithofacies boundaries from well log data (Baldwin *et al.* 1990; Rogers *et al.* 1992). The method has its inherent learning ability to map some relation between input and output space, even if, there is no explicit *a priori* operator linking the measured litho log properties to the well log response.

Roth & Tarantola (1994) applied ANN based inversion scheme to recover the velocity structure from the seismogram. They made several experiments to demonstrate the stability and effectiveness of ANN based inversion algorithms using the noisy geophysical records. They inferred that the ANN based method is not stable for analysing strongly correlated noisy geophysical signals. However, these researchers have concluded that the ANN could be used for solving the non-trivial inverse problem. Devilee *et al.* (1999) developed an efficient probabilistic ANN approach to solve inverse problem and applied it to determine the Eurasian crustal thickness by inverting the surface wave velocities. More recently Aristodemou *et al.* (2005) presented the result of inversion of well-logging data using neural networks. They have noted that in litho logical problems, the lithology/lithofacies are usually obtained from the borehole core data. However, when the core data are not available, the down hole geophysical logs can be used to infer the nature of the surrounding rocks (Benaouda *et al.* 1999). Alternatively, the trained networks can be used to interpret lithofacies at greater depth of drilled borehole of same geology.

Here, we develop a super self-adapting back propagation (SSABP) neural network program to classify lithofacies boundaries and apply the method to well log data from German Continental Deep Drilling Project (KTB). To demonstrate the effectiveness of this method, we compare our findings with existing results and also test its robustness in the presence of coloured noise in the data. These results would provide a better understanding of the crustal inhomogeneity and structural discontinuity over the KTB region.

KTB DATA

The German Continental Deep Drilling Project (KTB) explores a metamorphic complex in northeastern Bavaria, southern Germany (Fig. 1).

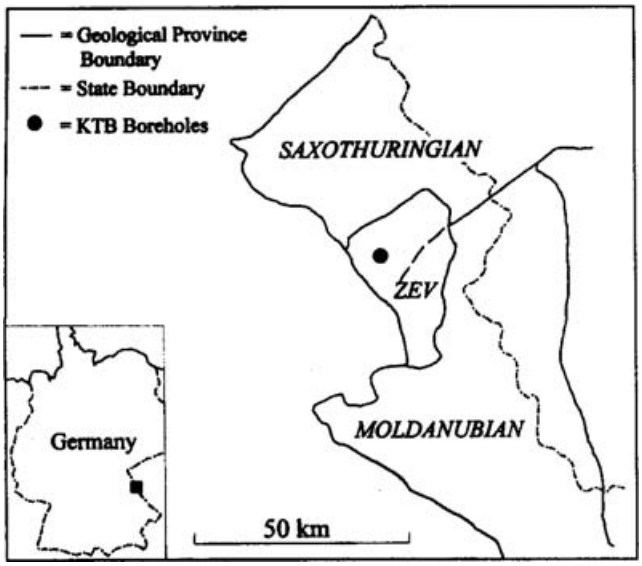

Figure 1. Location map of the KTB boreholes, Saxothuringian, Moldanubian, and ZEV (Erbendorf-Vohenstraub zone) represent the main geological units of the region (after Leonardi & Kümpel 1999).

Lithologically, the continental crust at the drill site consists of three main facies units: paragneisses, metabasites and alternations of gneiss-amphibolites, with minor occurrence of marbles, calc-silicates, orthogeneisses, lamprophyres and diorites (Berckhemer *et al.* 1997; Emmermann & Lauterjung 1997; Pechnig *et al.* 1997; Leonardi & Kümpel 1998, 1999) (Fig. 2). The detailed information about the KTB data and its geophysical significance has been well discussed in several earlier papers (Berckhemer *et al.* 1997; Emmermann & Lauterjung 1997; Pechnig *et al.* 1997; Leonardi & Kümpel 1998, 1999). A brief summary of the data pertinent to this study is, however, presented here to preserve self-sufficiency of the paper. Total depth of the main hole and pilot hole are 9101 and 4000 m, respectively. The borehole data are sampled at 0.1524 m (6 in.) intervals. These records are complete, continuous and uninterrupted series and hence could be utilized for the classification of the lithofacies units.

We parameterized here three sets of recorded well log data (viz., gamma ray, density and neutron porosity) to constrain the lithofacies boundaries. Due to the chemical composition, gamma ray activity exhibits a general increase from the most mafic rocks (ultramafites) to the most acidic rocks (potassium-feldspar gneisses). Hence, total gamma ray is the most important parameter for differentiating the metamorphic succession. In general, amphibolites and metagabbros, which are the main rock types of the massive metabasite units, are physically characterized by lower gamma ray activity and higher density than the rocks of the paragneisses sections. This is related to the mineral content, which within metabasites consists of more mafic and dense minerals like hornblende and garnet biotite. Paragneisses are composed mainly of quartz, plagioclase and micas. Since pore space in the crystalline basement is very low, neutron porosity response is found to be dependent upon the mineralogical composition. Enhanced porosity is, in general, restricted to discrete zones of faulting and fracturing, however, neutron porosity in undisturbed depth sections is predominantly reacting to the water bound minerals like phyllosilicates or amphiboles. Hence, rock type's poor in these minerals, such as quartz and feldspar-rich gneisses show very low neutron porosities. In contrast, rocks with high phyllosilicate

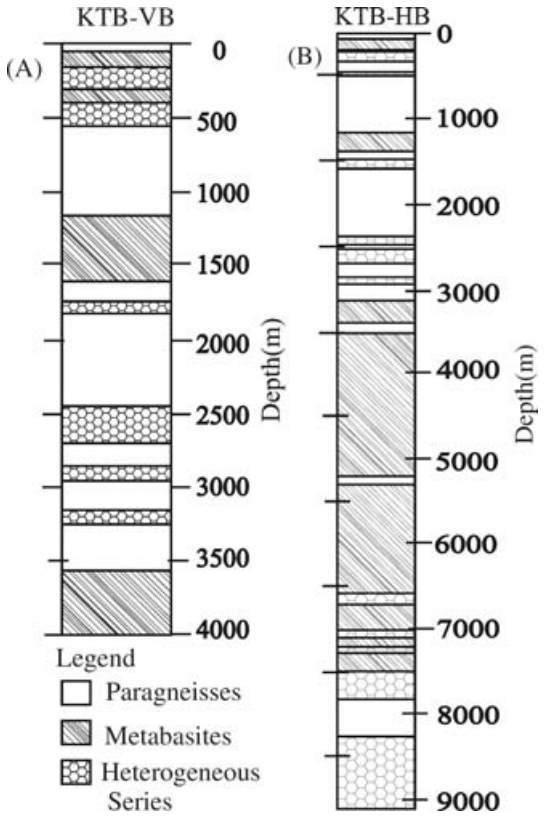

Figure 2. Reference diagram of lithofacies section of KTB (A) pilot hole (KTB-VB) (B) main hole (KTB-HB) (after Emmermann & Lauterjung 1997).

and amphibole contents produce striking increases in the neutron porosity.

THE MULTILAYER PERCPTRON (MLP)

ANN configuration and a brief mathematical background

ANNs form a class of non-linear computational systems that attempt to mimic the natural behaviour of biological neurons (Rosenblatt 1958) (Fig. 3a). Fig. 3(c) depicts the graphical representation of input and target vectors, for example, density (g/cc), porosity (per cent) and gamma ray (A.P.I.), which are randomly derived from Table 1. Apparently one can visualize that distribution patterns of the well log data depicted in Fig. 3(c) is complex and weakly non-linear and hence a multilayer neural network model with monotonically increasing activation functions could be appropriately applied for the classification of lithofacies. MLPs are special configurations of ANN that are most powerful methods for solving the non-linear classification and boundaries detection problems. In general, architecture of a MLP consists of one input layer, one output layer and at least one intermediate hidden layer between input and output. In a fully connected MLP, neurons of each layer are connected to the neurons of the next layer through weight. As depicted in figure (Fig. 3a), the input layer constitutes the input data for the nodes in hidden layer and the output data of this hidden layer constitutes the input for the output layer. There is no connection between nodes in the same layer.

The most widely used back-propagation (BP) training phase begins by sending the input values through the network and computing

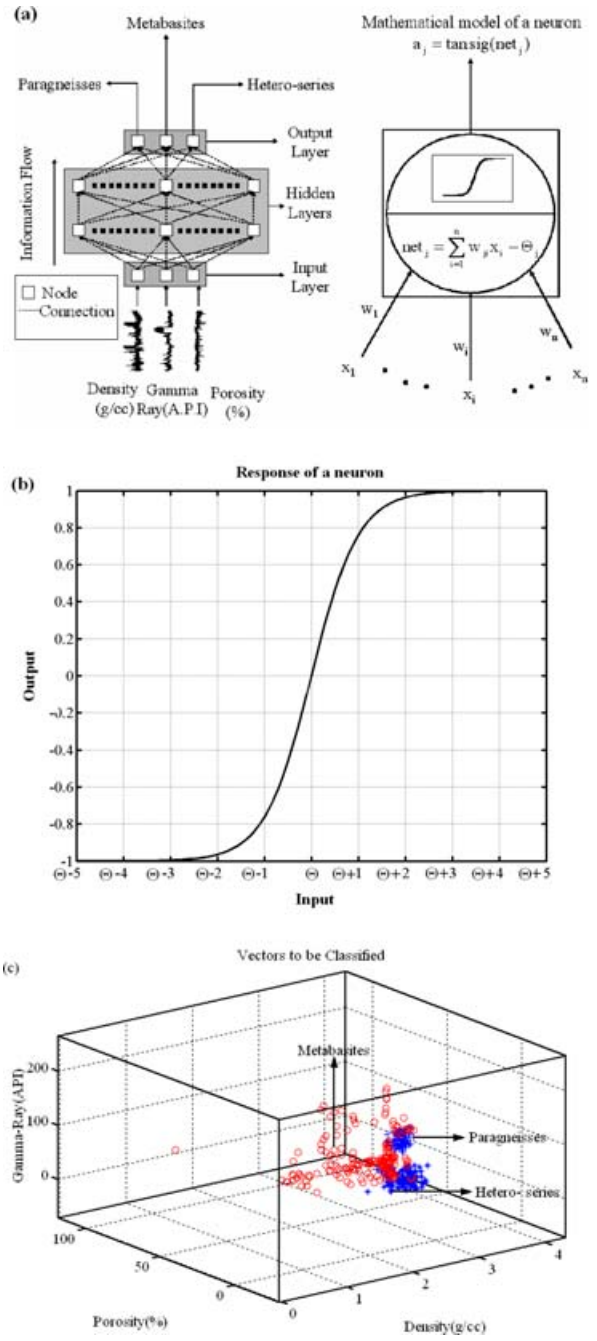

Figure 3. (a) Layout of four layer neural network with bottom layer containing three nodes each taking three well log parameters, here density (g/cc), porosity (per cent) and gamma ray (A.P.I.), two intermediate/hidden layer which are fully connecting between bottom layer/input layer and output layer (left), and mathematical expression of a neuron (right). 'x' represents input and subscript 'i' represents the number of nodes in the input layer. At each node of the hidden layer the net arguments are squashing through a non-linear activation function of type hyperbolic tangent where w_{ji} represents the connection weight between the ith node in the input layer and the jth node in the hidden layer. (b) Typical response of a non-linear activation function of type hyperbolic tangent. When the sum of the argument of a neuron is comparable to the threshold value Θ_j it squashes linearly, otherwise it saturates with value $+1$; -1 gives non-linearity for non-linear mapping between input and output space. (c) Plot of input vector containing density (g/cc), porosity (per cent) and gamma ray (A.P.I.) and target vector of our perceptron. Obviously, from the well log data, the lithofacies is not fully linearly separable.

© 2007 The Authors, *GJI*, **169,** 733–746
Journal compilation © 2007 RAS

Table 1. Showing the significant limits to generate forward model for neural network training indicating that gamma ray intensity value most crucial factor to categorize lithofacies unit in metamorphic area.

Lithofacies unit	Density (g/cc)	Neutron porosity (per cent)	Gamma ray intensity (A.P.I)	Desired output (binary code)
Paragneisses	2.65–2.85	5–15	70–130	100
Metabasites	2.75–3.1	5–20	0–50	010
Heterogeneous Series	2.60–2.9	1–15	40–90 and 120–190	001

the deviation of the calculated output vectors from the true ones. The next step consists of propagating the deviation (error) between computed and desired output vectors backward to adjust the weighting coefficients, so that error could be minimized (Rumelhart *et al.* 1986) (Fig. 4a). More explicitly, let $net_j^{(l)}$ be a value (output) received by the jth node in layer (l), $w_{ji}^{(l)}$ be a connection weight between the ith node in layer ($l-1$) and jth node in layer (l) and x_i be an input variable for ith node in layer ($l-1$). The $net_j^{(l)}$ can be formally represented as

$$net_j^{(l)} = \sum_{i=1}^{n} w_{ji}^{(l)} x_i^{(l-1)} - \Theta_j^{(l)}, \tag{1}$$

where, $\Theta_j^{(l)}$ and $net_j^{(l)}$ represent, respectively, the bias unit and weighted sum for the jth node in layer (l). The output depends on the weighted sum of an input vector and a weight vector. The sum may not fall on an optimal part of the curve so one way to ensure that it does is to add a bias to the sum to shift it left or right along the curve (Poulton 2001) (Fig. 3b). The output of the jth node in layer (l) is passed through non-linear transfer function, which can be written as (Benaouda *et al.* 1999)

$$a_j^{(l)} = f_j\left(net_j^{(l)}\right). \tag{2}$$

We used here the commonly used non-linear hyperbolic tang sigmoid transfer function of the form of

$$f_j\left(net_j^{(l)}\right) = \frac{e^{\beta(net_j^{(l)})} - e^{-\beta(net_j^{(l)})}}{e^{\beta(net_j^{(l)})} + e^{-\beta(net_j^{(l)})}}. \tag{3}$$

Here, e denotes the basis of the natural logarithm (Fig. 3b), β is a constant which determines the stiffness of the function near $net_j^{(l)} = 0$ in layer (l) (Roth & Tarantola 1994). The value of β is adopted as 1.0 to keep the sigmoidal function in shape (Wasserman 1993).

In order to understand the procedure more explicitly in a mathematical sense, let us assume that E represents the network's global error functions. The local error e at the jth node in the layer (l) is computed as: (Benaouda *et al.* 1999)

$$e_j^{(l)} = -\frac{\partial E}{\partial (net_j^{(l)})} = f_j'(net_j^{(l)}) \sum_k e_k^{(l+1)} w_{kj}^{(l+1)}. \tag{4}$$

The goal of the learning process is to minimize the network's global error function by modifying the connection weights by Δw_{ji}. This is done by using the gradient descent rule as follows:

$$\Delta w_{ji}^{(l)}. = -\eta_{ji}^{(l)} \left(\frac{\partial E}{\partial w_{ji}^{(l)}}\right). = \eta_{ji} e_j^{(l)} x_i^{(l-1)}, \tag{5}$$

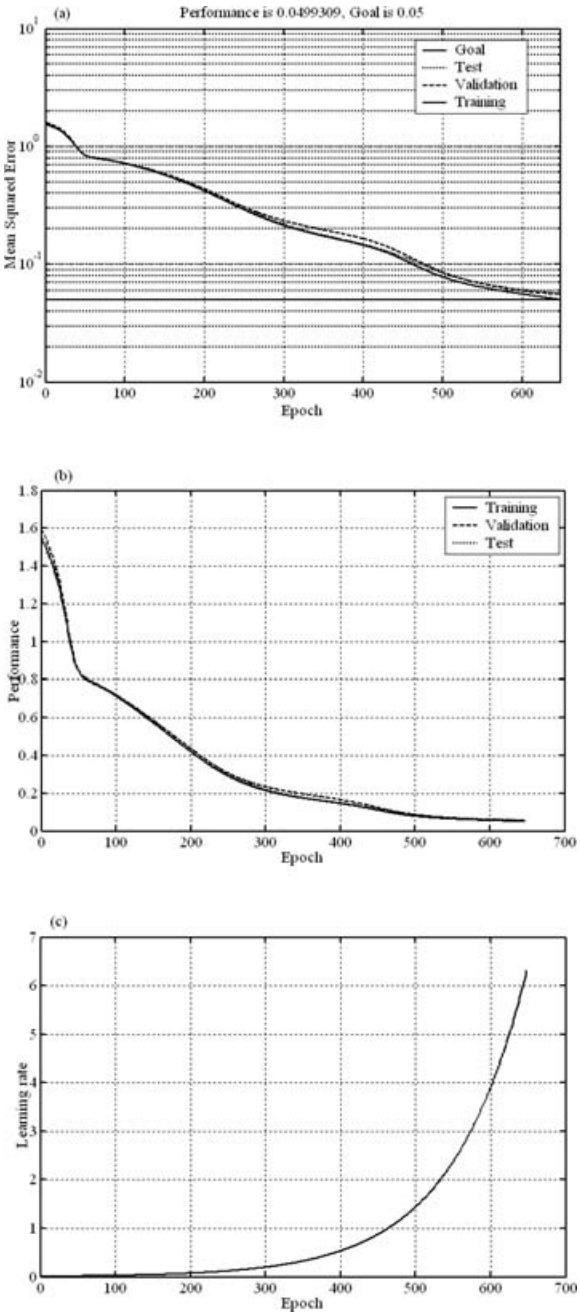

Figure 4. (a) Training history/progress of neural network with gradient descent with momentum and self/variable adaptive learning rate back propagation. Initial mean square error was 1.54688. After 648 epochs the network reaches below the error tolerance 0.05. (b) Performance function on three sets of data: training, validation and testing. The sets suggest that the overall performance is consistent along the error surface. (c) Shows the relation between epoch and learning rate.

© 2007 The Authors, *GJI*, **169,** 733–746
Journal compilation © 2007 RAS

where $\eta_{ji}^{(l)}$ is learning rate at layer (l). (Benaouda *et al.* 1999) The global error function used here is of the form of

$$E = \frac{1}{2}\sum_j (D_j - O_j)^2, \tag{6}$$

where D_j and O_j are, respectively, the desired and the actual output at each node in the output layer.

Super self adaptive back propagation (SSABP)

It is well known that the global error is highly non-linear function of the weights and biases and, therefore, may introduce many local minima in the error surface. The back propagation algorithms (BPA), which are based on the error correction rule, have been used for optimization of the network's global error by modifying the connection weights based on the knowledge of local error at each node (Rumelhart *et al.* 1986; Wasserman 1993; Bishop 1995; Poulton 2001). In many cases, however, the networks solution becomes trapped in one of these local minima. The SSABP paradigm implemented here uses momentum and adaptive learning rate, which speed up the network training and smoothes the error function during the training process and thereby avoids local minima (Hecht-Nielsen 1991). The learning rate is made responsive to the complexity of the local error surface and weights are updated at each epoch using current learning rate. Here an epoch equals to one presentation for every training sample (i.e. one pass through the training set). In a mathematical term the connections weights, with momentum m are updated as follows

$$\Delta w_{ji}^{(l)}(t+1) = \eta_{ji}^{(l)} e_j^{(l)} x_i^{(l-1)} + m\Delta w_{ji}^{(l)}(t), \tag{7}$$

where t is a time index, since weight change on the right hand side is old with respect to the left-hand side in eq. (7). An adaptive learning rate keeps the learning step size as large as possible while maintaining the progress of learning stable (Figs 4a and b). In SSABP (Wasserman 1993), each weight w_{ji} has an associated step size (learning rate) η_{ji}. As with the momentum, if the new error exceeds the old error by more than a predefined ratio, new weight and biases are automatically discarded. Also step size is decreased as η_{down} for that weight setting which can be mathematically presented as

$$\eta_{ji}^{(l)}(t+1) = \eta_{ji}^{(l)}(t)\eta_{\text{down}} \tag{8}$$

and if the new error is less than the old error, the step size is increased as η_{up} setting,

$$\eta_{ji}^{(l)}(t+1) = \eta_{ji}^{(l)}(t)\eta_{\text{up}}. \tag{9}$$

Initially, many sets of weight values were chosen randomly and set between -1 and $+1$. To start with the program, the learning rate η and momentum m are chosen as $\eta = 0.01$ and $m = 0.9$, respectively. In the SSABP algorithm, the changes in η are multiplicative rather than additive and thereby it makes the growth rate stepwise exponential (Fig. 4c) rather than linear. We note that the values of two constants are problem dependent (Wasserman 1993) and hence in order to avoid instability, it is necessary to limit the maximum value of η. For this we have used $\eta_{\text{up}} = 1.01$ and $\eta_{\text{down}} = 0.70$ that are best suited to our classification problem. Computational procedure is developed in such a way that adaptive learning rate increases or decreases automatically only to the extent that the network could be trained without large surface errors and resumes stable learning (Figs 4b and c).

Probabilistic approach of boundaries identification

Several workers have used histogram types of networks for classification problems (Dowla *et al.* 1990; McCormack *et al.* 1993). In the present study, we used a network, which is defined and discussed in detail in a recent work of Devilee *et al.* (1999). Accordingly, for each set of inputs, (e.g. density, neutron porosity and gamma ray intensity), the trained networks return the probable occurrence of outputs corresponding to the three classes of lithofacies and not the actual values of density, porosity and gamma ray. The following solution approximately satisfies the constraint:

$$\sum O_j = 1. \tag{10}$$

The output of last layer of the network can be written as,

$$O_j = P(lith_j). \tag{11}$$

Here, $lith_j$ defines lithofacies number j ($j = 1,\ 2,\ 3$) and P represents posterior probability. Output value can be interpreted in terms of posterior probability distributions (Devilee *et al.* 1999). Following Benaouda *et al.* (1999), let us assume that ($P_1 = N_1/N, \ldots \ldots P_k = N_k/N$) are, respectively, *a priori* probabilities (where N_i is the number of elements in the ith class and N is the total number of elements in the data) and the probability distribution of a sample $X = (X_1, \ldots, X_m)$ is known for each class j ($j = 1, \ldots, K$), denoted as $f_j(X)$. The posterior probability distribution of X belonging to the jth class is given by Bayes' rule .

$$P\langle j|X\rangle = \frac{P_j f_j(X)}{\sum_{i=1}^{K} P_i f_i(X)}. \tag{12}$$

Thus, Bayes' rule representing the relation between posterior and *a priori* distribution is used to assign the sample X to a class that has the largest posterior probability greater than a certain threshold value. The trained histogram network approximates the posterior probabilities of X belonging to one of the three lithologies as stated in eq. (12). The probability density $f_j(\cdot)$; $j = 1, \ldots\ldots K$ can be calculated by non-parametric method based on the observed samples. The maximum likelihood value corresponds to the class with maximum posterior probability, which is obtained from neural network output as follows: in ideal case, if the lithofacies of a particular class exists, the output value of the node in the last layer is 1 or very close to 1 and if not, it is 0 or very close to 0.

MODEL INITIATION AND IMPLEMENTATION

Hidden layers, connection weights and output

Cybenko (1989) showed that MLPs are universal approximators and could approximate asymptotically any continuous function using a single hidden layer. However, there is no firm convention or theoretical limit for optimizing the number of hidden layers or number of neurons in each hidden layer (Benaouda *et al.* 1999). Some empirical rules, however, have been discussed in literature (Lippman 1987; Pulli & Dysart 1990) that provides some criteria for choosing the number of hidden layers and neurons as a function of the input and output neurons. In the present model, the input layer consists of three nodes and accepts input values from density (g/cc), neutron porosity (per cent) and gamma ray intensity (A.P.I.) data. We used two hidden layers each consisting of fifteen individual nodes that are best suited to the present classification problems as depicted by the well log data

© 2007 The Authors, *GJI*, **169,** 733–746
Journal compilation © 2007 RAS

(Fig. 3a). These are fully connected across layers by non-linear function expressed in terms of the nodal input variables and connection weights (Fig. 3a). The output layer consists of three nodes to represent the occurrence of three possible lithofacies units, for example, paragneisses, metabasites and heterogeneous series. Heterogeneous series also contains alteration of gneiss-amphibolites, with minor occurrence of marbles, calcsilicates, orthogeneisses, lamprophyres and diorites (Berckhemer *et al.* 1997; Emmermann & Lauterjung 1997; Pechnig *et al.* 1997; Leonardi & Kümpel 1998, 1999).

Number of training samples

Table 1 shows the published results of core sample analysis from the KTB site (Pechnig *et al.* 1997). We have randomly generated 702 representative input/output pairs within the bounds defined in Table 1 for the ANN training. It may be noted that the limited number of training sets were generated here to have a comparative status with the published histogram. The training set is used to train the MLP that is to update the weights and biases for each node by the self-adaptive error back-propagation method.

Designing a network with appropriate number of internal variables (weights and biases) is vital for avoiding the overfitting problem. Several workers have suggested that this problem could be avoided, to some extent, by taking more training samples than the internal variables (Baum & Haussler 1989; Van der Baan & Jutten 2000). Following Van der Baan & Jutten (2000) the internal variable (N) for the present MLP structure can be calculated as follow:

$$N \approx [(N_i + 1)N_{h1} + (N_{h1} + 1)N_{h2} + (N_{h2} + 1)N_o \quad (13)$$

Here, N_i (Input) = N_o (Output) = 3; Nh_1 (First hidden layer) = Nh_2 (Second hidden layer) = 15 (Fig. 3a). Application of this formula to our designed network yields $N \approx [(3 + 1) \times 15 + (15 + 1) \times 15 + (15 + 1) \times 3)] \approx 342$ internal variables which is less than 351 input data being used for training. This gives justification for the correct MLP structure being used in the present analysis.

Input data scaling and model parameterization

Normalization of the raw data (input/output), before presenting it to the network is to avoid saturation. Hence, we scaled the input/output values between 0 and 1 [−1 and +1] by using a simple linear transformation algorithm, (Poulton 2001); normalized input = 2×(input-minimum input)/(maximum input-minimum input) − 1 (Fig. 3b). The training history is presented in Fig. 4(a). The training phase completed after about 4000 epochs for an arbitrarily assigned performance goal of (0.05). The minimum performance gradient falls below 10^{-15} (Fig. 4b). The initial error function, that is, mean square error (MSE) was found 1.54688, which is the value of sum-squared error (SSE) divided by the number of patterns in the training file. Here SSE is defined as the sum of the squares of the difference between the target output and network output over all nodes for all patterns. Although these values may not be the unique one, the chosen parameters (e.g. epochs, performance goal and gradient) enabled the fast and efficient training for the present case.

Data division, model validation and testing

Overfitting is one of the severe drawbacks in ANN modelling. This refers to the fact that the selected training set is memorized in such a way that performance is only excellent on this set but not on other data leading to the useless predictive model. Hence, one of the most important considerations in the ANN training is to avoid overfitting and have good generalization. For this, we used early stopping to increase the generalization capacity of ANN. The stopping criteria depend upon achieving the best-fitting model beyond which there would not be any appreciable change in the error function. In this approach, the available data is shuffled appropriately and partitioned into three random subsets. The first 50 per cent of the total data set is used for training. The remaining 50 per cent were used for examining the generalization capability of the trained network. Here, again the 24.93 per cent (i.e. 175) data were kept for validation and remaining 25.07 per cent (i.e. 176) for testing (Fig. 4a). The validation set is not explicitly presented during the training phase but the error on the validation set is monitored during this process. The MLP error on validation set is calculated at the same time and training is stopped when it reaches a minimum. This cross-validation scheme prevents the network from memorizing the training set and provides the best generalization. The testing is used to quantify the MLP predictions/model performances once the weight and biases are frozen. We rechecked the different partitions manually and performed the testing and validation to avoid any possibility of overfitting during the training process. In all our experiments we observed that the network was getting overfit after 648 epochs with error value of 0.05 (Fig. 4a).

Generalization capacity of the network

Performance of the trained network can be evaluated by error analysis on the validation and test data sets. Error deviation is difference between the target (binary output target, 1,0,0 for pargneisses, 0,1,0 for metabasites and 0,0,1 for heteroseries) and the actual network output of the input log data. Fig. 5(a) shows the result of error deviations on validation data set (left) and test data set (right) pertaining to paragneisses, metabasites and heterogeneous series. As can be clearly seen the accuracy of validation data set corresponding to paragneisses, metabasites and heterogeneous series is considerably good. Comparatively, however, paragneisses and metabasites exhibit better accuracy than heterogeneous series. Similarly, for the test samples (right) accuracy for metabasites series is better than paragneisses, and heterogeneous series. Overall the average accuracy of the network prediction/generalization corresponding to the three lithofacies units is very good.

NETWORK SENSITIVITY TO CORRELATED NOISE

In many geological/geophysical situations, it has been observed that some kind of deceptive correlated (red) noise dominates the field observations and corrupts the signal. It is also true that no data can be totally noise free, as there will always be some unknown source of noise inherently creeping in the data. We do not have an exact idea about the per cent of noise present in our well log data. However, assuming that there is some possibility of inescapable noise in our data, we thought it appropriate to test the robustness of our analysis and stability of the result. For this, we generated correlated noise using the first order autoregressive model of the form of $X(t) = AX(t - 1) + \varepsilon_t$. In this model new generated values depend on the immediately preceding values with some additive random component (Fuller 1976). Here, $X(t)$ is a stationary time series at time t and ε_t is the Gaussian white noise with zero mean and unit variance. A is a constant representing the maximum likelihood estimator, which is determined from the input data. The maximum likelihood values

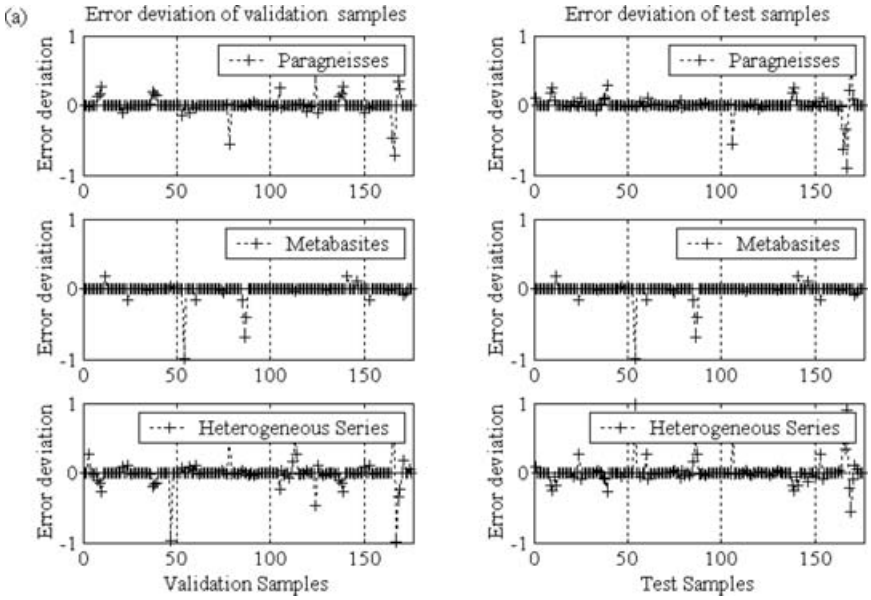

Figure 5. Error deviation of validation set data (left) and test data (right) pertaining to paragneisses, metabasites and heterogeneous series (a) when the input generalization set is noise free. (b) When the input generalization set is corrupted with 30 per cent red noise (c) When the input generalization set is corrupted with 50 per cent red noise.

for the validation data set is estimated as 0.52 for density, 0.21 for porosity and 0.53 for gamma ray and for the test data set 0.47 for density, 0.23 for porosity and 0.55 for gamma ray. The model results are presented in Table 2, which show the percentages of accuracy for the validation data set corresponding to paragneisses, metabasites and heterogeneous series for different levels (5–50 per cent) of correlative red noise. The error deviations for 30 and 50 per cent correlated noise in the input log data are displayed in Figs 5(a)–(c). The present results suggest that the predictive capability of the network is considerably good for those data sets, which are contaminated with red noise up to a certain limit (i.e. to 20 per cent or so), however the predictive capability is not so robust with strongly correlated noise. The present model experiment also agrees well with the view of Roth & Tarantola (1994) who have applied neural network based inversion method to the recorded seismogram mixed with various kinds of noises in attempt to recover the velocity structure.

Regression analyses

A regression analysis verifies the accuracy of the overall performance of the network. For such an analysis, a set of training data is normalized and the network is trained and simulated using the normalized data. Now the output of the network is unnormalized using the algorithm unnormalized input = 0.5 × (normalized input + 1) × (maximum input–minimum input) + minimum input (Poulton 2001). Following this procedure, we performed linear regression analysis between the network outputs and the targets to check the quality of the network training. We performed a regression analysis on the network that we have previously trained by applying early stopping method. Here, we pass the network output and the corresponding targets through the regression program, which is developed here. It returns three parameters. The first two parameters u and v correspond to the slope and the y-intercept of the best linear regression fit relating to the network output (A) and target (T), respectively. The network outputs are plotted against the targets (T), which are shown as open circles in Figs 6(a)–(c). A dashed line indicates the best linear fit (slope 1 and y-intercept 0). The solid line in the above figure shows the perfect fit (output equal to target). The third variable is the correlation coefficient (R) between the network outputs and the targets, which is a measure of how well the variation in the output is explained by the targets. If this number is equal to 1, there is perfect correlation between targets and outputs. The results of the linear regression analysis for the total set of data sets corresponding to paragneisses, metabasites and heterogeneous series are given in Table 3 and are displayed in Figs 6(a)–(c). The results indicate that slope (a), correlation coefficient (R) and y-intercept (b) are very close to 1, 1 and 0, respectively, which suggest that the performance of the trained network is very good.

COMPARISON OF ANN MODEL RESULT WITH THE PUBLISHED RESULT

The published results of lithofacies successions (Emmermann & Lauterjung 1997) are redrawn (Fig. 2) for the sake of clarity. Maximum Likelihood Geologic Section (MLGS) derived from the ANN modelling for both KTB boreholes is also drawn and compared with published subsections (Figs 7 and 8). These results, both pilot and main bore hole, are displayed in Figs 7 and 8 at 500 m data windows. The above figures exhibit the posterior probability distribution in a 3-coloumns grey-shaded matrix with black representing 1 and white representing 0 (Figs 7a–h and 8a–f).

Pilot bore hole (KTB-VB) (up to 4000 m depth)

The present result based on the SSABP model confirms, in general, the presence of paragneisses, metabasites and heterogeneous series within the first 500 m data window. However, a close examination and comparison of the model results with the published results exhibit a somewhat poor correlation (Fig. 7a). For instance, for depth ranging from 30 to 100 m depths below the surface, the model shows the presence of heterogeneous series, instead of paragneisses. Similarly, for the depth ranging from 240 to 250 m,

© 2007 The Authors, *GJI*, **169,** 733–746
Journal compilation © 2007 RAS

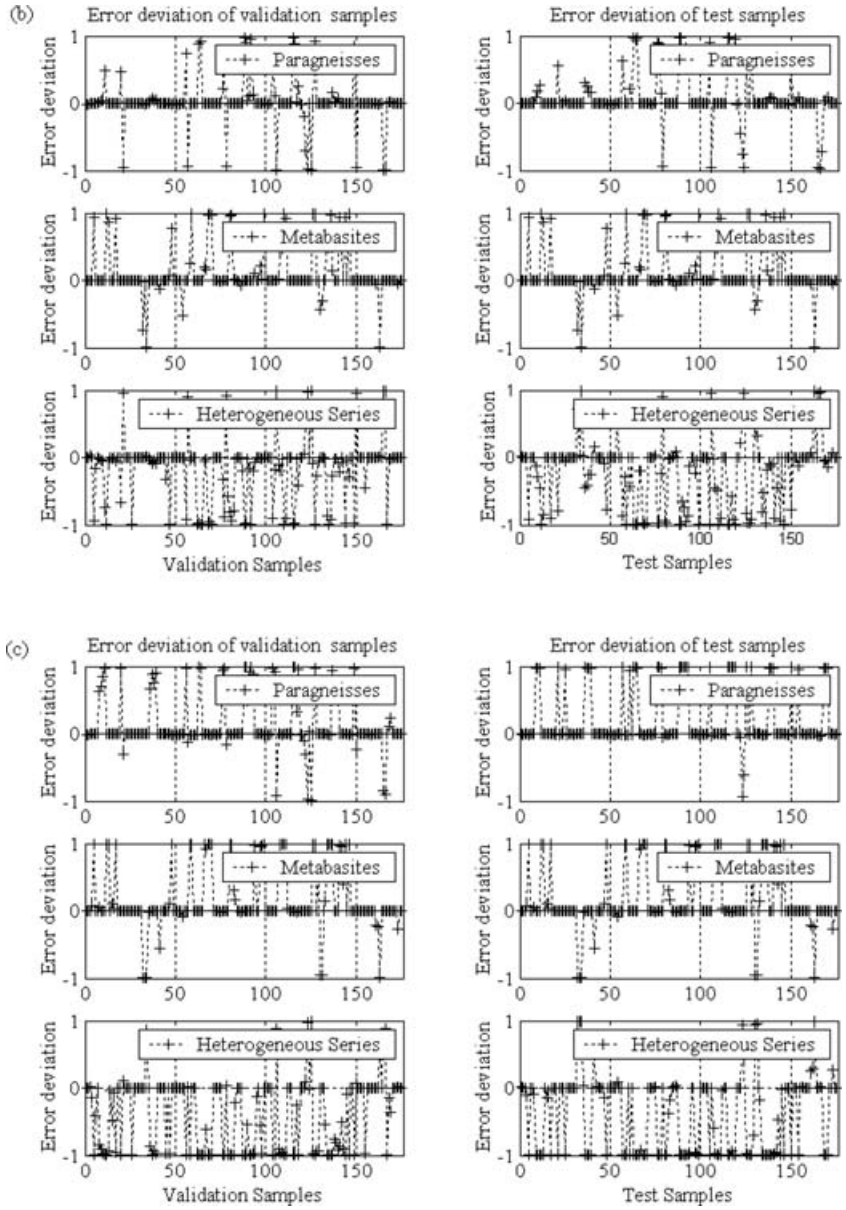

Figure 5. (*Continued*).

Table 2. Percentage of accuracy validation and test data set with different red noise level.

Red noise level	Percentage of accuracy in generalization data set						
	Validation data set			Test data set			Average stability within plus or minus 5 per cent error limits
	Paragneisses	Metabasites	Heterogeneous series	Paragneisses	Metabasites	Heterogeneous series	
5 per cent	90.86 per cent	98.29 per cent	86.29 per cent	92.61 per cent	96.59 per cent	88.09 per cent	92.12 per cent
10 per cent	90.86 per cent	96.57 per cent	84.00 per cent	92.05 per cent	94.89 per cent	86.36 per cent	90.78 per cent
20 per cent	85.71 per cent	86.29 per cent	69.14 per cent	85.80 per cent	79.55 per cent	62.50 per cent	78.16 per cent
30 per cent	80.57 per cent	82.29 per cent	60.00 per cent	75.00 per cent	76.70 per cent	51.14 per cent	70.95 per cent
40 per cent	75.43 per cent	74.29 per cent	49.86 per cent	73.33 per cent	74.43 per cent	47.23 per cent	65.76 per cent
50 per cent	74.29 per cent	76.57 per cent	46.86 per cent	76.76 per cent	69.89 per cent	46.59 per cent	65.16 per cent

the model result shows the presence of paragneisses instead of heterogeneous series. Still below, depths ranging from 305 to 340, 400 to 430 and 430 to 490 m the modelling results show presence of paragneisses heterogeneous series and metabasites instead of heterogeneous series; metabasites, instead of heterogeneous series and paragneisses instead of heterogeneous series, respectively. Comparison of the present result within the 500–1500 m depths below the surface with published results (Figs 7b–c) shows good conformity

Table 3. Illustrating the results of linear regression analysis of major three litho types.

Litho types	Correlation coefficient (R) between target (T) & network output (A)	Slope (u)	y-intercept of the best linear regression relating targets to network output (v)
Paragneisses class	0.964	0.898	0.0243
Metabasites class	0.984	0.976	0.0134
Heterogeneous series class	0.958	0.906	0.0404

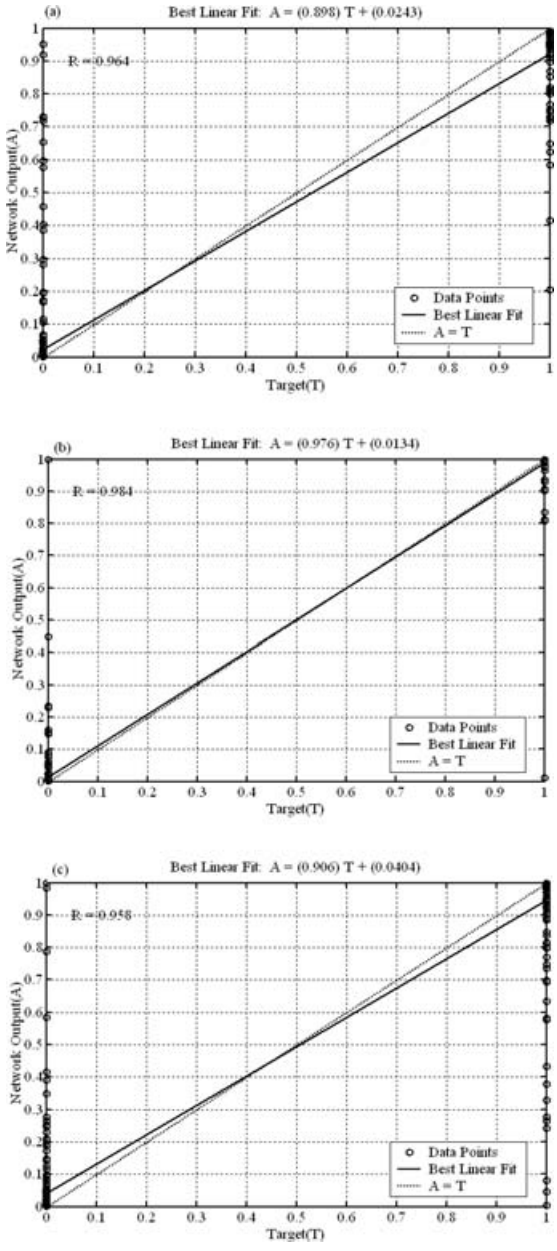

Figure 6. (a) Linear regression analysis of total set of data corresponding to paragneisses. Correlation coefficient (R) between target (T) and network output (A) is 0.892, slope is 0.964, and y-intercept of the best linear regression relating targets to network is 0.02431. The network outputs are plotted versus the targets as open circles. A dashed line indicates the best linear fit. The perfect fit (output equal to targets) is indicated by the solid line. (b) Same as (a) for metabasites yielding a correlation coefficient 0.984, slope 0.976, and y-intercept 0.0134. (c) Same as (a) for heterogeneous series yielding a correlation coefficient 0.958, slope 0.906, and y-intercept 0.0404.

with the three lithofacies successions, for example, paragneisses, metabasites and heterogeneous series. However, within this interval there is some dissimilarity too. Our result for depth intervals 520–556, 579– 582, 598–601, 707–712 and 1145–1168 m suggest, respectively, the presence of paragneisses instead of heterogeneous series, heterogeneous series instead of paragneisses, heterogeneous series instead of paragneisses, heterogeneous series instead of paragneisses and metabasites instead of paragneisses. The present result also show good matching within the depth interval ranging from 1500 to 2500 m (Figs 7d–e) except for the presence of heterogeneous series from depth 1597 to 1618 m; paragneisses from depth 1744 to 1817 and 2442 to 2467 m. Our result shows that paragneisses layers mostly dominate within the depth interval of 2500–3000 m mostly revealing the presence of paragneisses from depth 2562 to 2623 m and from 2852 to 2953 m interbedded with a finer thin metabasites structures corresponding to a depth range of 2640 to 2646 m. (Fig. 7f). Fig. 7(g) exhibits the presence of paragneisses class and heterogeneous series, which are consistent with the published results except for the depth 3408–3421 m. In addition to this, our results also suggest the presence of paragneisses class and heterogeneous series in depths intervals ranging from depths 3204 to 3248 and 3409 to 3418 m, respectively. Comparison of the present result in the depth range of 3500–4000 m (Fig. 7h) shows a succession of paragneisses and metabasites, which is identical to the published results. The minor deviations and some differences observed between published and the present result is explained in Section 'Discussion'.

Main bore hole (KTB-HB) (up to 7000 m depth)

Comparison of the SSABP result of the main KTB bore hole data exhibits, in general, good correlation with the published results of Emmermann & Lauterjung (1997) (Figs 8a–d). There is some dissimilarity also. For instance, there is evidence of bimodal combination of heteroseries and metabasites sequence within depth interval of 4400–4500 m instead of only single depositional sequence of metabasites as reported in previous investigation. Further there is evidence of three thinner heterogeneous series at depth intervals ranging from 4580 to 4583, 4809 to 4812 and 4580 to 4583 m instead of a single metabasites unit. Again within depth interval of 5440–5500 m there is evidence of bimodal sequence of heteroseries and metabasites instead of metabasites only. Further, a closer look of the above figures reveal the presence of heterogeneous series, metabasites and paragneissess from depth 5500 to 5650 m instead of only metabasites and presence of heterogeneous series from depth 5820 to 5840 m instead of metabasites unit. It is interesting to note here that the SSABP modelling results also reveals successions of additional structures at depth intervals ranging from 6017 to 6026, 6322 to 6334 and 6400 to 6418 m in heterogeneous series (Fig. 8e) classification, in addition to the main classes at a depth interval from

© 2007 The Authors, *GJI*, **169,** 733–746
Journal compilation © 2007 RAS

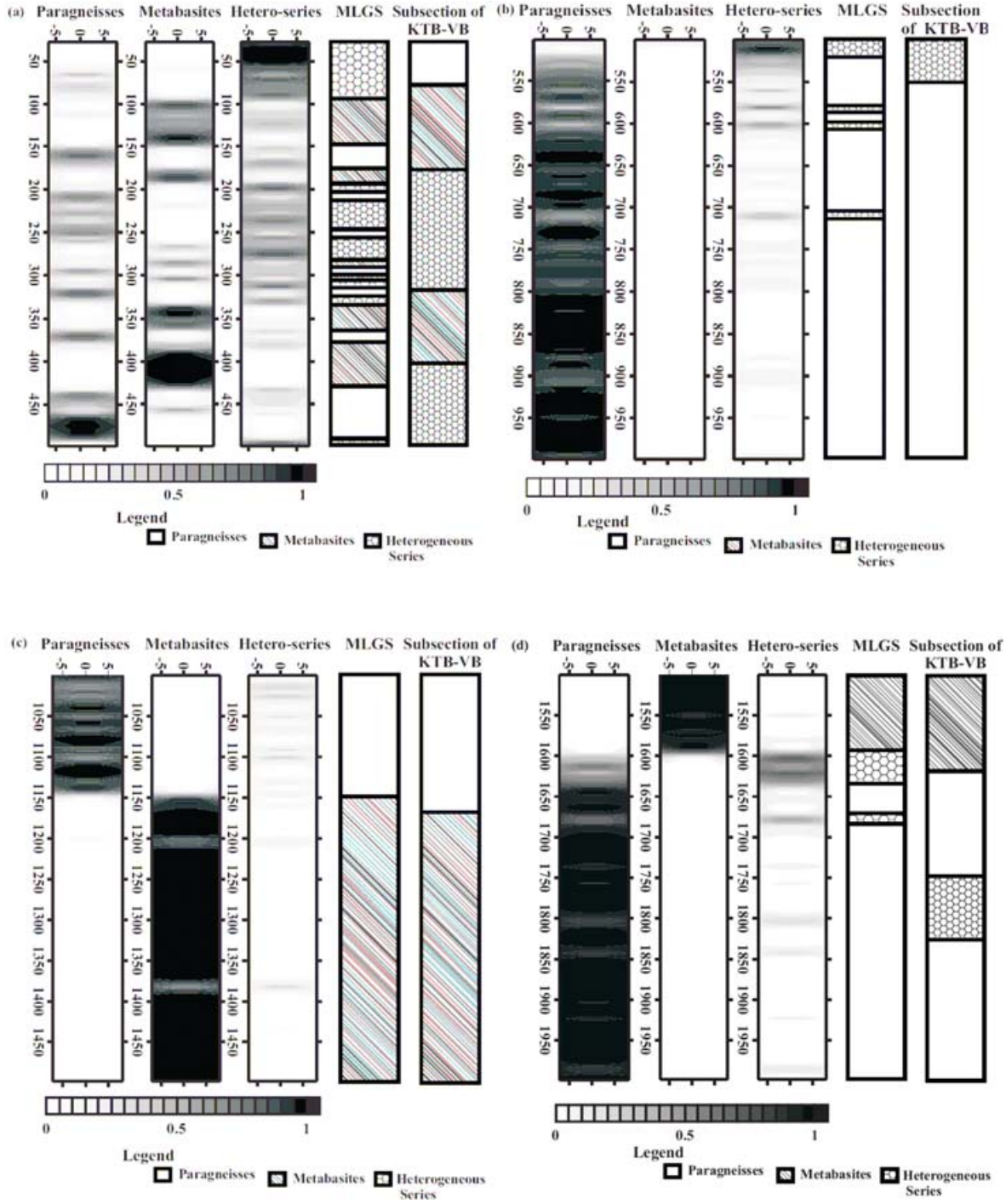

Figure 7. (a) Comparison of the Maximum Likelihood Geological Section (MLGS) from neural network approach (left) with published lithofacies subsection of pilot hole (KTB-VB) (right; after Emmermann & Lauterjung 1997) for depth interval 0–500 m. In this interval 0–28 m data is not available. (b)–(h) Same for depth ranges 500–1000, . . . , 3500–4000 m in KTB pilot hole(KTB-VB).

5543 to 5560 m (Fig. 8d). Fig. 8(f) shows dominance of heterogeneous series. However, our result shows presence of heterogeneous series from depth 6550 to 6665 m instead of metabasites and heterogeneous series and presence of heterogeneous series and metabasites at depth interval of 6710–7000 m instead of only metabasites unit.

DISCUSSIONS

Comparison of MLGS with published lithospecies section of Emmermann & Lauterjung (1997) (Figs 7 and 8) exhibits more or less matching patterns that are well correlated. In addition to this, the SS-ABP model also reveals some finer structural details, which seem to

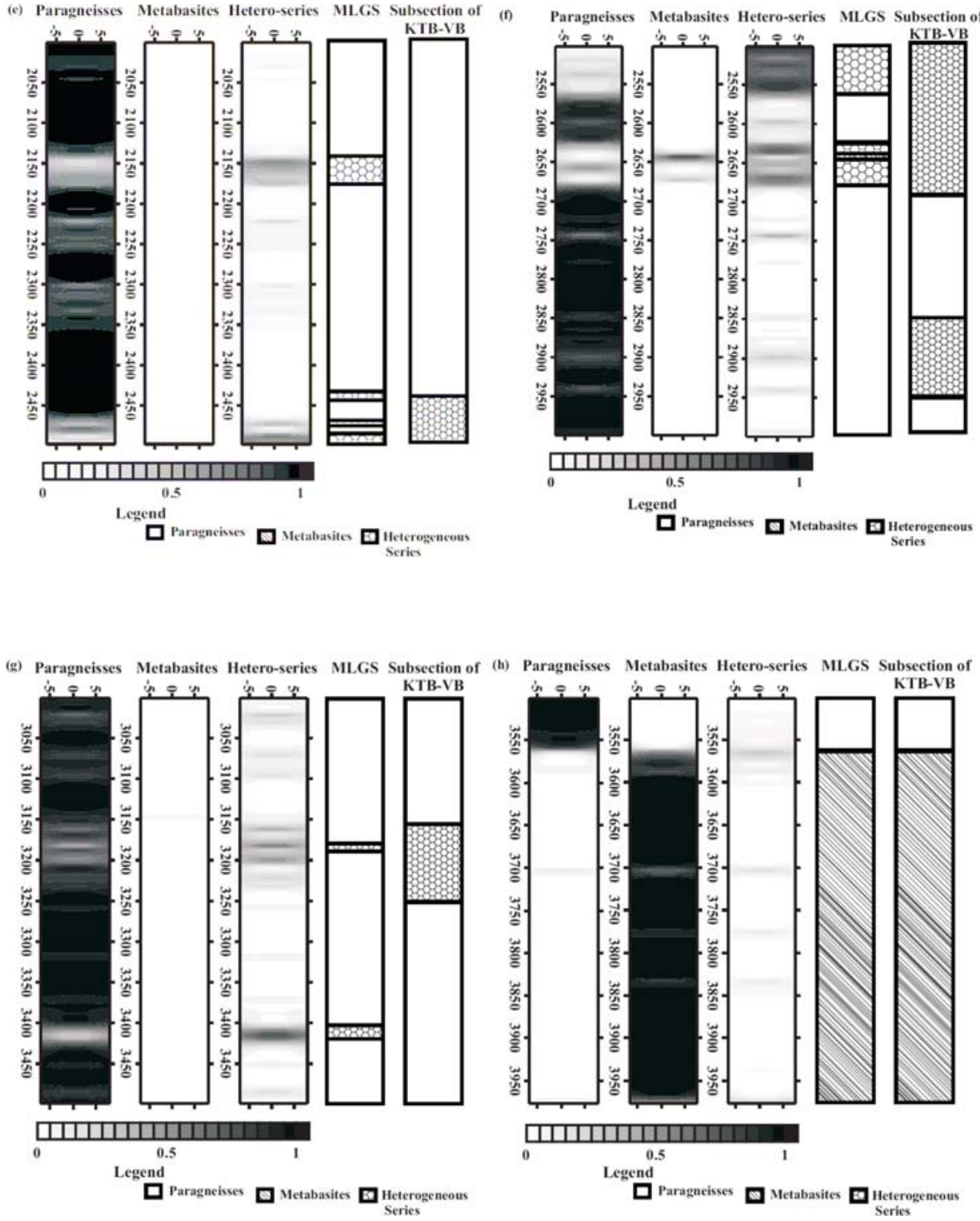

Figure 7. (*Continued*).

be geologically significant. We note, however, that in complex non-linear geological situations, such as the one being analysed here, it is somewhat difficult to assert an exact geological interpretation as to whether these apparently visible finer details inferred from our study, are truly meaningful geological structures or simply an artefact of analysis. Just for the sake of our curiosity and, of course, to examine the authenticity of these structural details, we manually checked a few samples produced by the trained network (Table 4). To our surprise the trained network produced more or less identical results that are consistent with the training data. It may be mentioned, however, that the present probabilistic histogram model of lithofacies classification cannot be uniquely constrained and/or compared with the existing litho section (Fig. 2), since the published results are mostly gross-average depth of the litho section. Secondly, the observed data may be also biased by deceptive 'red' noise signals with non-zero mean and might contain additional error due to limitations in the KTB data resolution. Some deviations between the two results are, therefore, expected. It is significant to mention,

© 2007 The Authors, *GJI*, **169,** 733–746
Journal compilation © 2007 RAS

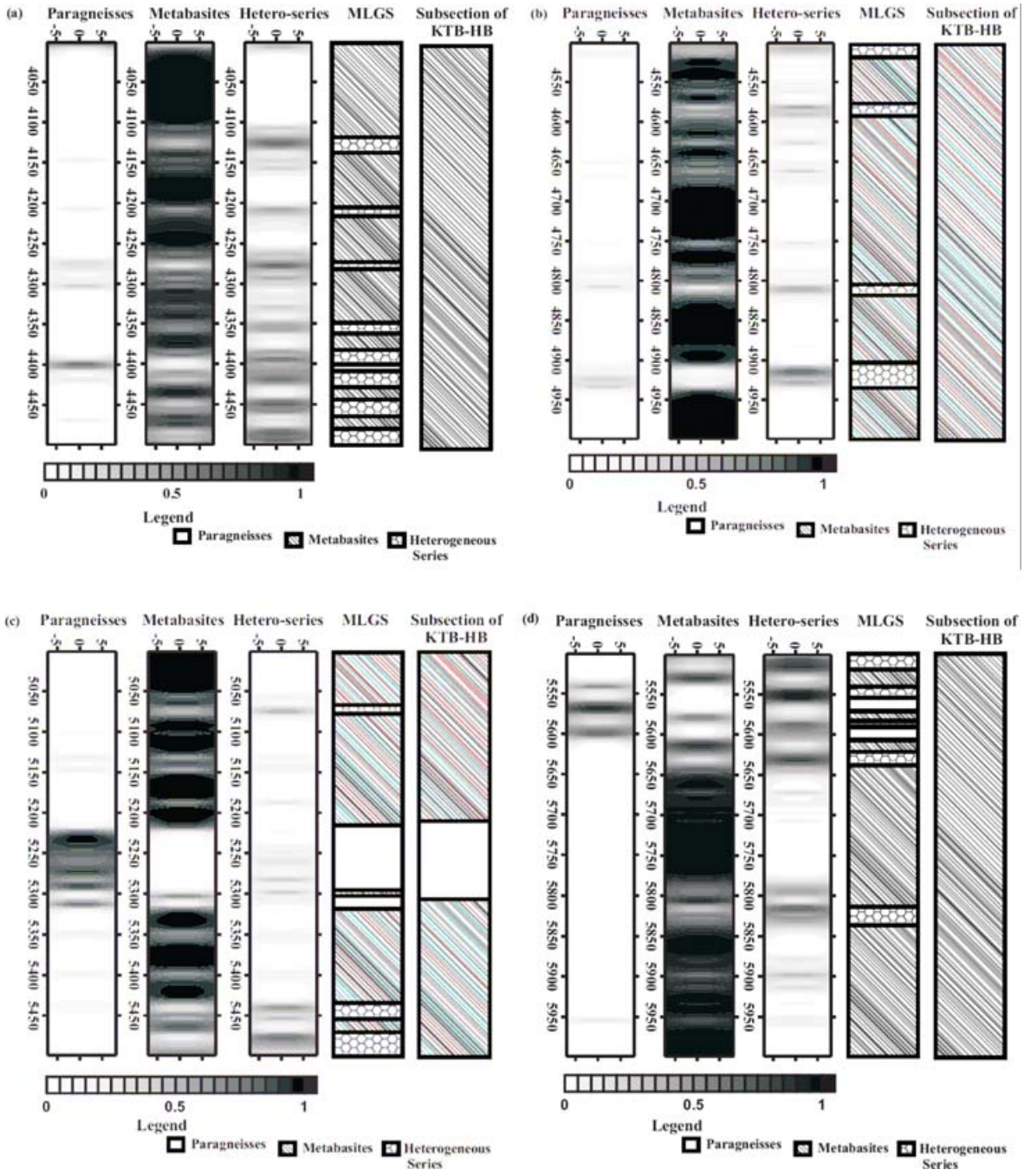

Figure 8. (a) Comparison of the Maximum Likelihood Geological Section (MLGS) from neural network approach (left) with published lithofacies subsection of main hole (KTB-HB) (right; after Emmermann & Lauterjung 1997) for depth interval 4000–4500 m. (b)–(f) Same for depth ranges 4500–5000 m, . . . , 6500–7000 m in KTB main hole(KTB-HB).

however, that most of the deviations and differences between the published results and the SSABP model results are observed in pilot bore hole, that too in the upper part of the crust. Further some of the deviations/mismatches between the present model result and published data apparently visible in some of the cases, might also arise due to uncertainty in terms of probability distributions, when winner node value is not significantly higher than the non-winner node values. We note, however, that while interpreting prediction of the network's output node with the maximum likelihood value, in most of the cases as discussed above, we found excellent separation between the wining and non-winning output node values rendering the actual patterns that are showing considerably high correlation coefficients ∼0.9687 (Table 3). Thus it may be emphasized that the SSABP algorithm, as developed here, combined with its validation test and regression analyses do provide credence to the authenticity of these results. Hence apparently visible finer details are not an artefact of either choosing the maximum likelihood value or due to any other reason rather they, in fact, are the inter-bedded geological structures that remained unrecognized in previous visual interpretation. The output of the histogram type networks for choosing maximum likelihood value, as discussed by Devilee *et al.* (1999), provides better guidance.

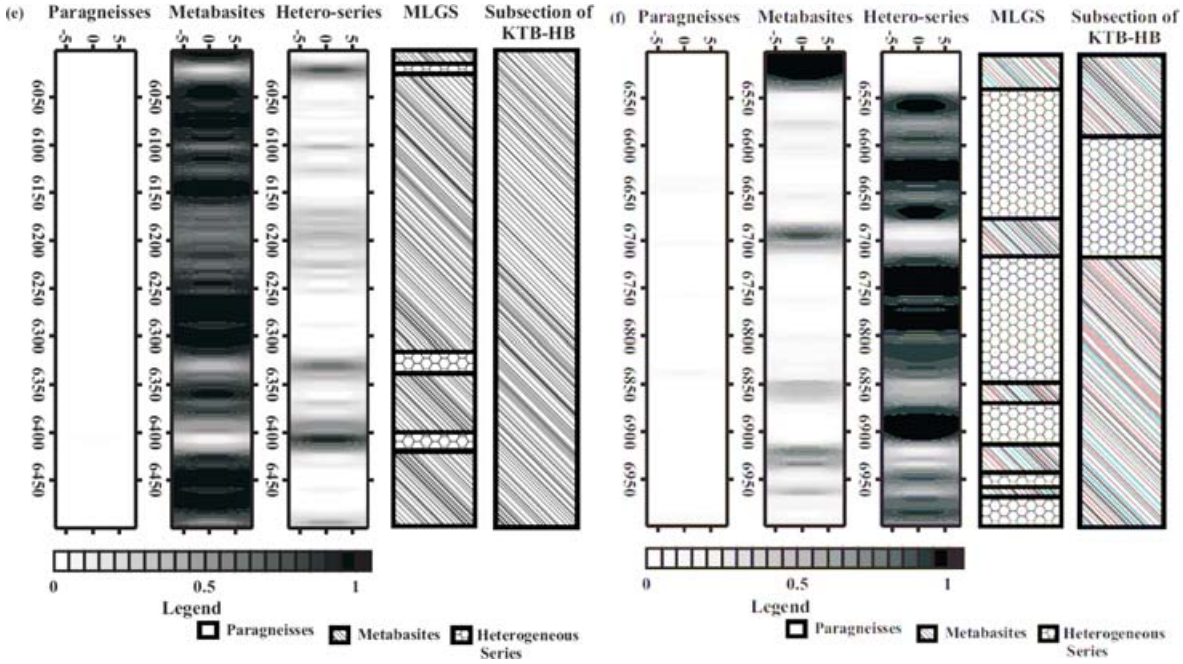

Figure 8. ((*Continued*)).

Table 4. Analysis of real data taken from both KTB pilot hole (KTB-VB) and KTB main hole (KTB-HB) from different depth.

Bore Hole (samples of data taken)	Depth (m)	Density (g/cc)	Neutron porosity (per cent)	Gamma ray intensity (A.P.I.)	Desired output (binary code)			Neural networks actual output		
KTB-VB	3119.171	2.719	10.805	107.1	1	0	0	0.998	0.000	0.001
KTB-VB	1574.292	2.940	12.343	45.007	0	1	0	0.004	0.999	0.000
KTB-VB	89.0016	2.736	10.46	82.050	0	0	1	0.472	0.000	0.835
KTB-VB	305.866	2.946	14.062	32.614	0	1	0	0.002	0.999	0.000
KTB-VB	893.826	2.824	12.946	128.41	0	0	1	0.314	0.000	0.680
KTB-VB	1393.546	3.017	11.24	23.268	0	1	0	0.003	0.999	0.000
KTB-VB	2252.472	2.809	14.949	119.17	1	0	0	0.974	0.000	0.017
KTB-VB	3864.254	2.948	13.591	19.107	0	1	0	0.002	0.999	0.000
KTB-VB	3559.454	2.746	12.11	104.35	1	0	0	0.998	0.000	0.001
KTB-HB	4007.206	2.867	14.122	45.596	0	1	0	0.002	0.996	0.007
KTB-HB	4505.554	2.634	11.522	29.91	0	1	0	0.000	0.979	0.031
KTB-HB	4808.677	2.625	15.443	84.418	0	0	1	0.051	0.000	0.994
KTB-HB	6325.362	2.755	15.727	13.359	0	1	0	0.001	0.999	0.000
KTB-HB	6515.862	3.004	14.823	20.325	0	1	0	0.002	0.999	0.000
KTB-HB	6807.099	2.742	11.174	55.444	0	0	1	0.001	0.009	0.982
KTB-HB	5504.231	2.914	15.514	33.633	0	1	0	0.001	0.999	0.000

CONCLUSIONS

A super self-adapting back propagation (SSABP) neural network program is developed and successfully applied to classify the lithofacies boundaries by using the well log data from the German Continental Deep Drilling Project (KTB). Besides providing additional finer evidence of the crustal inhomogeinity on KTB site, the result also supports the existing results. This provides a good testimony to use the SSABP based techniques to solve the problems of borehole geophysics. The main conclusions of this analysis are follows:

(i) The SSABP neural network technique is an efficient and cost-effective tool to interpret large amount of borehole log data. The SSABP based technique is also robust to analyse modestly correlated noisy data.

(ii) A comparative study of the present model results with the published result suggests that the SSABP method is also able to model the succession of some finer structures, which were hitherto not recognized. Such findings may have implications in understanding the crustal inhomogeneity.

(iii) Because of its computational efficiency, it is proposed that the present methods can be further exploited for analysing large number of borehole data in other areas of interest.

(iv) Finally, some deviations observed in SSABP neural network analysis from the prior knowledge seem to be interesting and should provide a basis for more detailed examination of the geological significance of finer structures intervening bigger geological units.

© 2007 The Authors, *GJI*, **169,** 733–746
Journal compilation © 2007 RAS

ACKNOWLEDGMENTS

We are indebted to the anonymous reviewers for their constructive comments and useful suggestions on our paper, which have improved in this form. We are also extremely grateful to the editor for his valuable suggestions and encouragements to revise the manuscript. We are also thankful to all staff member of editorial office for his or her cooperation to improve the manuscript. One of the authors Saumen Maiti (SM) expresses sincere thanks to Council of Scientific and Industrial Research (C.S.I.R) for providing the Research Intern Awards to carry out his research work. Ralf Gelfort gave helpful comments on earlier version of this manuscript. SM and RKT are also thankful to Dr V. P. Dimri, Director, National Geophysical Research Institute, Hyderabad for his kind permission to publish this work.

REFERENCES

Aristodemou, E., Pain, C., Oliveira, C. & Goddard, T., 2005. Inversion of nuclear well-logging data using neural networks, *Geophys. Prospect,* **53,** 103–120.

Baldwin, J., Bateman, A.R.M. & Wheatley, C.L., 1990. Application of neural network to the problem of mineral identification from well logs, *The Log Analyst,* **31,** 279–293.

Baum, E.B. & Haussler, D., 1989. What size network gives valid generalization?, *Neural Comp,* **1,** 151–160.

Benaouda, D., Wadge, G., Whitmarsh, R.B., Rothwell, R.G. & MacLeod, C., 1999. Inferring the lithology of borehole rocks by applying neural network classifiers to downwhole logs: an example from the Ocean Drilling Program, *Geophys. J. Int.,* **136,** 477–491.

Berckhemer, H. *et al.*, 1997. Petrophysical properties of the 9-km deep crustal selection at KTB, *J. geophys. Res.,* **102**(B8), 18 337–18 361.

Bishop, C.M., 1995. *Neural Networks for Pattern Recognition*, Oxford University Press, New York.

Boadu, F., 1998. Inversion of fracture density from field seismic velocities using artificial neural networks, *Geophysics,* **63,** 534–545.

Busch, J.M., Fortney, W.G. & Berry, L.N., 1987. Determination of lithology from well logs by statistical analysis, *SPE Formation Evaluation,* **2,** 412–418.

Calderon-Macias, C., Sen, M.K. & Stoffa, P.L., 2000. Artificial neural networks for parameter estimation in geophysics, *Geophys. Prospect.,* **48,** 21–47.

Coppola, E.A. Jr., Rana, A.J., Poulton, M.M., Szidarovszky, F. & Uhl, V.W., 2005. Aneural network model for predicting aquifer water level elevations, *Ground Water,* **43**(2), 231–241.

Cybenko, G., 1989. Approximation by superpositions of sigmoidal function, *Math. Control, Signals Systems,* **2,** 303–314.

Dai, H. & Macbeth, C., 1995. Automatic picking of seismic arrivals in local earthquake data using an artificial neural network, *Geophys. J. Int.,* **120,** 758–774.

Delfiner, P., Peyret, O. & Serra, O., 1987. Automatic determination of lithology from well logs, *SPE Formation Eval.,* **2,** 303–310.

Devilee, R.J.R., Curtis, A. & Roy-Chowdhury, K., 1999. An efficient probabilistic neural network approach to solving inverse problems: Inverting surface wave velocities for Eurasian crustal thickness, *J. geophys. Res.,* **104**(12), 28 841–28 856.

Dowla, F.U., Talor, S.R. & Anderson, R.W., 1990. Seismic discrimination with artificial neural networks: preliminary results with regional spectral data, *Bull. seism. Soc. Am.,* **80,** 1346–1373.

Dysart, P.S. & Pulli, J.J., 1990. Regional seismic event classification at the NORESS array: seismological measurements and use of trained neural network, *Bull. seis. Soc. Am.,* **80,** 1910–1933.

Emmermann, R. & Lauterjung, J., 1997. The German Continental Deep Drilling Program KTB: overview and major results, *J. geophys. Res.,* **102,** 18 179–18 201.

Feng, X.-T., Seto, M. & Katsuyama, K., 1997. Neural dynamic modeling on earthquake magnitude series, *Geophys. J. Int.,* **128,** 547–556.

Franke, W., 1989. The geological framework of the KTB drill site, in *The German Continental Deep Drilling Program (KTB)*, pp. 38–54, eds Emmermann, R. & Wohlenberg, J., Springer, Berlin.

Fuller, W.A., 1976. *Introduction to Statistical Time Series*, John Wiley and Sons, New York.

Gassaway, G.R., Miller, D.R., Bennett, L.E., Brown, R.A., Rapp, M. & Nelson, V., 1989. *Amplitude variations with Offset: fundamentals and Case Histories*, SEG Continuing Education Course Notes.

Hecht-Nielsen, R., 1991. *Neurocomputing*, Addison-Wesley Publishing Co., USA.

Helle, H.B., Bhatt, A. & Ursin, B., 2001. Porosity and permeability prediction from wireline logs using artificial neural networks: a North Sea case study, *Geophys. Prospect.,* **49,** 431–444.

Huang, Z., Shimeld, J., Williamson, M. & Katsube, J., 1996. Permeability prediction with artificial neural network modeling in the Venture gas field, offshore eastern Canada, *Geophysics,* **61,** 422–436.

Leonardi, S. & Kümpel, H., 1998. Variability of geophysical log data and signature of crustal heterogeneities at the KTB, *Geophys. J. Int.,* **135,** 964–974.

Leonardi, S. & Kümpel, H., 1999. Fractal variability in super deep borehole-implications for the signature of crustal heterogeneities, *Tectonophysics,* **301,** 173–181.

Lippman, R.P., 1987. An introduction to computing with neural networks, *IEEE ASSP,* **4,** 4–22.

McCormack, M.D., Zaucha, D. & Dushek, D., 1993. First break refraction event picking and seismic data trace editing using neural networks, *Geophysics,* **58,** 67–78.

Murat, M.E. & Rudman, A.J., 1992. Automated first arrival picking: A neural network approach, *Geophys. Prospect.,* **40,** 587–604.

Pechnig, P., Haverkamp, S., Wohlenberg, J., Zimmermann, G. & Burkhardt, H., 1997. Integrated interpretation in the German Continental Deep Drilling Program: Lithology, porosity, and fracture zones, *J. geophys. Res.,* **102,** 18 363–18 390.

Pickett, G.R., 1963. Acoustic character logs and their application in formation evaluation, *J. Petr. Tech.,* **15,** 659–667.

Poulton, M., Ed., 2001. *Computational Neural Networks for Geophysical Data Processing*, Pergamon, Amsterdam.

Pulli, J.J. & Dysart, P.S., 1990. An experiment in the use of trained neural networks for regional seismic event classification, *Geophys. Res. Lett.*, **17,** 977–980.

Raiche, A., 1991. A pattern recognition approach to geophysical inversion using neural nets, *Geophys. J. Int.,* **105,** 629–648.

Rogers, S.J., Fang, J.H., Karr, C.L. & Stanley, D.A., 1992. Determination of lithology from well logs using a neural network, *Am. Ass. Petrol. Geol. Bull.,* **76**(5), 731–739.

Rosenblatt, F., 1958. The perceptron: a probabilistic model for information storage and organization in the brain, *Psycholog. Rev.,* **65,** 386–408.

Roth, G. & Tarantola, A., 1994. Neural networks and inversion of seismic data, *J. geophys. Res.,* **99,** 6753–6768.

Rumelhart, D.E., Hinton, G.E. & Williams, R.J., 1986. Learning representations by back-propagating errors, *Nature,* **323,** 533–536.

Saggaf, M.M., Okzos, M.N. & Mustafa, H.M., 2003. Estimation of reservoir properties from seismic data by smooth neural networks, *Geophysics,* **68,** 1969–1983.

Van der Baan, M. & Jutten, C., 2000. Neural networks in geophysical applications, *Geophysics,* **65,** 1032–1047.

Wasserman, P.D., 1993. *Advanced Methods in Neural Computing*, Van Nostrand Reinhold, New York.

Wolff, M. & Pelissier-Combescure, J., 1982. FACIOLOG: automatic electrofacies determination: SPWLA Annual Logging Symposium paper FF, 6–9.

Yin-ju, B., 2002. Application of genetic BP network to discriminating earthquakes and explosions, *Acta Seism. Sinica,* **15,** 540–549.

Zhan, L., Poulton, M.M. & Wang, T., 2002. Borehole electrical resistivity modeling using neural networks, *Geophysics,* **67**(6), 1790–1797.